

Transfer of BECs through discrete breathers in an optical lattice

H. Hennig^{1,2,3}, J. Dornig^{3,4} and D. K. Campbell³

¹*Max Planck Institute for Dynamics and Self-Organization, Göttingen, Germany*

²*Institute for Nonlinear Dynamics, University of Göttingen, Germany*

³*Boston University, Boston, MA 02215, USA and*

⁴*Laboratoire de Physique Théorique et Astroparticules,
CNRS-IN2P3-UMR5207, Université Montpellier 2, 34095 Montpellier, France*

(Dated: May 6, 2022)

We study the stability of a stationary discrete breather (DB) on a nonlinear trimer in the framework of the discrete nonlinear Schrödinger equation (DNLS). In previous theoretical investigations of the dynamics of Bose-Einstein condensates in leaking optical lattices, collisions between a DB and a lattice excitation, e.g. a moving breather (MB) or phonon, were studied. These collisions lead to the transmission of a fraction of the incident (atomic) norm of the MB through the DB, while the DB can be shifted in the direction of the incident lattice excitation. Here we show that there exists a total energy threshold of the trimer, above which the lattice excitation can trigger the destabilization of the DB and that this is the mechanism leading to the movement of the DB. Furthermore, we give an analytic estimate of upper bound to the norm that is transmitted through the DB. Our analysis explains the results of the earlier numerical studies and may help to clarify functional operations with BECs in optical lattices such as blocking and filtering coherent (atomic) beams.

PACS numbers: 67.85.De, 63.20.Pw, 03.75.Lm, 42.65.Tg

1. Introduction

Since the experimental realization of Bose-Einstein Condensation (BEC) of ultra-cold atoms in optical lattices (OLs) [1], many groups of researchers have achieved an extraordinary level of control over BECs in optical traps [2–5]. Among other important applications, this control has allowed for the investigation of analogues of complex solid state phenomena [6–10]. Technologically, the emerging field of “atomtronics” promises a new generation of nanoscale devices.

An important generic feature of nonlinear lattices is the existence of discrete breathers (DBs), which are spatially localized, time-periodic, stable (or at least long-lived) excitations in spatially extended perfectly periodic discrete systems [11–13]. DBs arise intrinsically from the combination of nonlinearity and the discreteness of the system. DBs have been observed in a variety of systems, including Josephson-junction arrays [14, 15], micromechanical systems [16], nonlinear waveguide arrays [17, 18], α helix proteins [19], spins in antiferromagnetic solids [20, 21] and BEC [6]. The existence, stability, and other properties of DBs have been studied theoretically throughout the last decade [13, 22–24]. Among other results, it was shown that they act as virtual bottlenecks which slow down the relaxation processes in generic nonlinear lattices [25–28].

Many theoretical studies of the dynamics of a BEC trapped in an OL use the discrete nonlinear Schrödinger equation (DNLS) to model the system. Several recent studies based on the DNLS have observed the collision of a stationary DB with a lattice excitation, e.g. a moving breather or phonon [27–29]. If the amplitude of the lattice excitation is too small, it is reflected entirely from the DB. Above a specific threshold amplitude, part of

the incident atomic norm is transmitted through the DB while the DB is destabilized and shifted by one or few lattice sites towards the incoming moving breather (MB) [48]. This transmission process plays a central role in the occurrence of scale-free atomic avalanches observed for a whole range of nonlinearities in leaking optical lattices [28]. However, this process has heretofore not been understood analytically.

In this article we analyze, analytically and numerically, the collision process of a stationary DB with a lattice excitation. To this end, we study the nonlinear trimer, i.e. the DNLS with $M = 3$ lattice sites (see e.g. [5] for an experimental realization of a similar system). We calculate analytically the threshold for the destabilization of the DB as well as an upper bound to the atomic norm that can be transmitted through the DB. The threshold and the transmission process are described by introducing a ‘Peierls-Nabarro energy landscape’ which restricts the accessible region of the phase space for excitations on the trimer. The ‘local Ansatz’, [30, 31], an approach applied successfully to studies of DBs on nonlinear lattices, suggests that the results we find for the trimer will apply to extended lattices; the agreement of our results with the recent numerical studies [28] confirms this. For the rather large nonlinearity we shall consider in the sequel, DBs are well localized, and the most basic and important DBs occupy only three sites. Within the local Ansatz we consider only the central site and the two neighboring sites of a DB. This allows us to reduce the high dimensional dynamical problem involving M sites to the nonlinear trimer. A detailed analysis of the reduced problem [30, 31] shows that (i) the DB corresponds to a trajectory in the phase space of the full system which is practically embedded on a two-dimensional toroidal manifold, thus being quasiperiodic in time; (ii) the full DB can be re-

produced accurately within the nonlinear trimer approximation.

Although we focus here on BECs, our results are also relevant in a wide range of other contexts in which the DNLS applies, most prominently coupled nonlinear optical waveguides [17, 18, 32–35].

2. The Model Hamiltonian

The Bose-Hubbard Hamiltonian is arguably the simplest model that captures the dynamics of a dilute gas of bosonic atoms in a deep optical lattice, with chemical potential small compared to the vibrational level spacing (see e.g. [3] for a review). In the case of weak interatomic interactions (superfluid limit) and/or a large number of atoms per well (so that the total number of atoms $N \sim \mathcal{O}(10^4 - 10^5)$ is much larger than the number of wells M), a further simplification is available since the BECs dynamics admits a semi-classical (mean-field) description. The resulting Hamiltonian describing the dynamics is

$$\mathcal{H} = \sum_{n=1}^M [U|\psi_n|^4 + \mu_n|\psi_n|^2] - \frac{J}{2} \sum_{n=1}^{M-1} (\psi_n^* \psi_{n+1} + c.c.), \quad (1)$$

where $n = 1, \dots, M$ is the index of the lattice site, $|\psi_n(t)|^2 \equiv N_n(t)$ is the mean number of bosons at site n (also referred to as the norm $N_n(t)$), $U = 4\pi\hbar^2 a_s V_{\text{eff}}/m$ describes the interaction between two atoms at a single site (V_{eff} is the effective mode volume of each site, m is the atomic mass, and a_s is the s -wave atomic scattering length), μ_n is the on-site chemical potential, and J is the tunneling amplitude. The “wavefunctions” ψ_n can be used as conjugate variables with respect to the Hamiltonian \mathcal{H} , leading to a set of canonical equations

$$\begin{aligned} i \frac{\partial \psi_n}{\partial \tau} &= \frac{\partial \mathcal{H}}{\partial \psi_n^*} \\ i \frac{\partial \psi_n^*}{\partial \tau} &= -\frac{\partial \mathcal{H}}{\partial \psi_n}, \end{aligned} \quad (2)$$

which upon evaluation yields the Discrete Nonlinear Schrödinger Equation

$$i \frac{\partial \psi_n}{\partial t} = \lambda |\psi_n|^2 \psi_n - \frac{1}{2} [\psi_{n-1} + \psi_{n+1}]. \quad (3)$$

Here, $\lambda = 2U/J$ is the nonlinearity and $t = J\tau$ is the normalized time. In Eq. 3 we have set $\mu_n = 0 \forall n$.

The DNLS can be applied to a remarkably large variety of systems, in particular this mathematical model describes (in the mean-field limit) the dynamics of a BEC in an OL of size M [36]. Experimentally, the tunneling rate J can be adjusted by the intensity of the standing laser wave field. A powerful tool to modify the on-site interaction U is via a Feshbach resonance, where the atomic interactions can be controlled over a large range simply

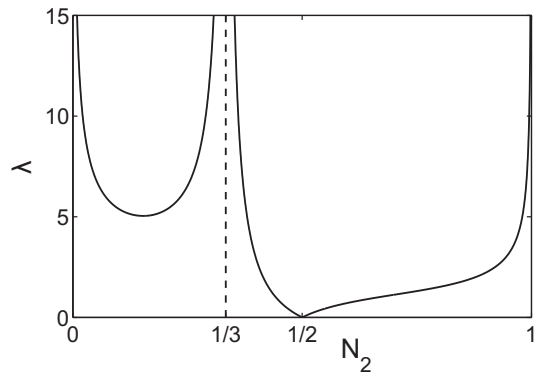


Figure 1: DB solutions for the symmetric case $\psi_1 = \psi_3$ (Eq. (7)). For a nonlinearity $\lambda > 5.04$ four symmetric solutions exist. The solution for $N_2 > 1/2$ is termed a bright breather, while the solution for $N_2 \rightarrow 0$ corresponds to a dark breather (see Eq. (12)). The dashed vertical line at $N_2 = 1/3$ marks the asymptote for the phase-wise and antiphase-wise time-periodic solutions for $\lambda \rightarrow \infty$.

by changing a magnetic field. A Feshbach resonance involves the coupling of free unbound atoms to a molecular state in which the atoms are tightly bound. When the energy levels of the molecular state and the state of free atoms come closer, the interaction between the free atoms increases. Thus, the nonlinearity λ can be varied experimentally. Here we will treat the repulsive case explicitly ($\lambda > 0$); however, the attractive case can be obtained via the ‘staggering’ transformation $\psi_n \rightarrow (-1)^n \psi_n$ followed by time-reversal $t \rightarrow -t$ [13].

3. Equations for the Nonlinear Trimer and Asymptotic Solutions

To analyze the transfer of norm through a DB (and related the stability of the DB) during a collision in the nonlinear trimer ($M = 3$) we begin with the equations

$$\begin{aligned} i \partial_t \psi_1 &= \lambda |\psi_1|^2 \psi_1 - \frac{1}{2} \psi_2 \\ i \partial_t \psi_2 &= \lambda |\psi_2|^2 \psi_2 - \frac{1}{2} (\psi_1 + \psi_3) \\ i \partial_t \psi_3 &= \lambda |\psi_3|^2 \psi_3 - \frac{1}{2} \psi_2. \end{aligned} \quad (4)$$

We normalize the wave functions such that the total atomic population reads

$$N = \sum_{n=1}^M |\psi_n|^2 = 1.$$

To find single frequency breather solutions in Eq. (4) for the symmetric case $\psi_1 = \psi_3$, we assume

$$\psi_n(t) = A_n e^{i\omega t}, \quad (5)$$

with amplitudes A_n and frequency w . This Ansatz, together with the conservation of particle number, leads to the set of equations

$$\begin{aligned} -wA_1 &= \lambda A_1^3 - \frac{1}{2}A_2 \\ -wA_2 &= \lambda A_2^3 - A_1 \\ 1 &= 2A_1^2 + A_2^2. \end{aligned} \quad (6)$$

Let us first calculate the relation between the (atomic) norm $N_2 = A_2^2$ at the central site and the nonlinearity λ . From Eq. (6), we find

$$\lambda(N_2) = \pm \frac{\sqrt{2}(2N_2 - 1)}{\sqrt{N_2(1 - N_2)}(3N_2 - 1)}. \quad (7)$$

We have four solutions above the bifurcation point at $\lambda \approx 5.04$ and two solutions for $0 \leq \lambda < 5.04$ (see Fig. 1). To gain further insight into the nature of the symmetric solutions in the trimer, we will revisit Eq. (6), which we convert into a quartic equation

$$x^4 + \frac{\lambda}{\sqrt{2}}x^3 - \sqrt{2}\lambda x - 1 = 0, \quad (8)$$

where

$$A_2 = \cos(\arctan(x)) = \frac{\text{sign}(x)}{\sqrt{1 + x^2}}. \quad (9)$$

Expansion of the exact real solutions of Eq. (8) in λ for the limiting case $\lambda \rightarrow 0$ gives

$$\begin{aligned} x_1 &= 1 + \frac{\lambda}{4\sqrt{2}} - \frac{5}{64}\lambda^2 + \mathcal{O}(\lambda^3) \\ x_2 &= -1 + \frac{\lambda}{4\sqrt{2}} + \frac{5}{64}\lambda^2 + \mathcal{O}(\lambda^3). \end{aligned} \quad (10)$$

At $\lambda=0$ the solution $\vec{\psi}(t) = (\psi_1(t), \psi_2(t), \psi_3(t))$ of Eq. (6) at time $t = 0$ reads $\vec{\psi}_{(x_1, x_2)}(0) = (1/2, \pm 1/\sqrt{2}, 1/2)$. The antisymmetric breather configuration $\vec{\psi}(0) = (-1/\sqrt{2}, 0, 1/\sqrt{2})$ is not included in our Ansatz, as we restrict ourselves to symmetric solutions.

Expansion around the limit $\lambda \rightarrow \infty$ leads to four real solutions

$$\begin{aligned} x_3 &= -\frac{1}{\sqrt{2}}\frac{1}{\lambda} - \frac{1}{4\sqrt{2}}\frac{1}{\lambda^3} + \mathcal{O}(\lambda^{-5}) \\ x_4 &= -\frac{1}{\sqrt{2}}\lambda + 2\sqrt{2}\frac{1}{\lambda} + 14\sqrt{2}\frac{1}{\lambda^3} + \mathcal{O}(\lambda^{-5}) \\ x_5 &= -\sqrt{2} - \frac{3}{2\sqrt{2}}\frac{1}{\lambda} - \frac{69}{16\sqrt{2}}\frac{1}{\lambda^2} + \mathcal{O}(\lambda^{-3}) \\ x_6 &= \sqrt{2} - \frac{3}{2\sqrt{2}}\frac{1}{\lambda} + \frac{69}{16\sqrt{2}}\frac{1}{\lambda^2} + \mathcal{O}(\lambda^{-3}). \end{aligned} \quad (11)$$

For infinite λ the solutions of Eq. (6) at time $t = 0$ are

$$\begin{aligned} \vec{\psi}_{(x_3)}(0) &= (0, 1, 0) \\ \vec{\psi}_{(x_4)}(0) &= (\sqrt{1/2}, 0, \sqrt{1/2}) \\ \vec{\psi}_{(x_5, x_6)}(0) &= (1/\sqrt{3}, \mp 1/\sqrt{3}, 1/\sqrt{3}), \end{aligned} \quad (12)$$

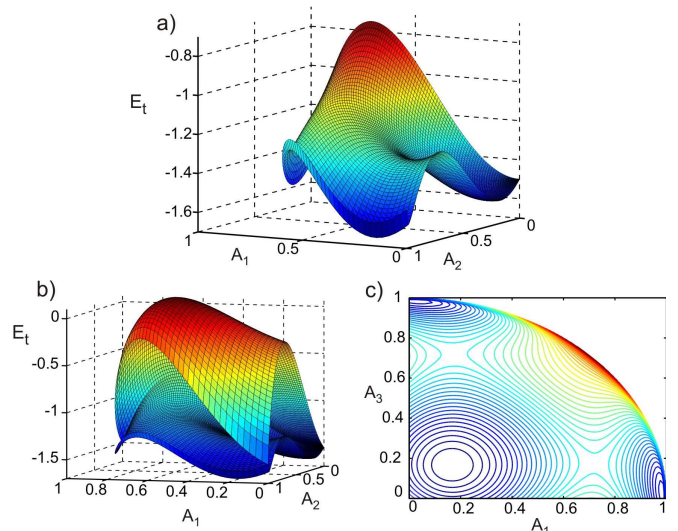


Figure 2: **(a)** The lower part of the PN energy landscape exhibits three minima separated by saddle points. **(b)** The phase space of the trimer is restricted to lie between the two parts of the PN shell, which consists of the lower and upper part of the PN landscape, which are shown in this panel. **(c)** Contour plot of (a), the lower part of the PN energy landscape. The three minima and saddle points are clearly visible. The minimum at $A_1 = A_3 = 0.17$ in (c) corresponds to the bright breather. The figure is plotted for $\lambda = 3$.

where the solution $\vec{\psi}_{(x_3)}$ is called a bright breather, $\vec{\psi}_{(x_4)}$ is named a dark breather (due to lack of norm at the central site) and $\vec{\psi}_{(x_5, x_6)}$ are phase-wise and antiphase-wise time-periodic solutions.

4. The Peierls-Nabarro energy landscape

Having found the symmetric DB solutions, we next focus on the transfer of norm through a bright breather, where the stability of the breather will play a crucial role. We start by introducing the concept of a ‘Peierls-Nabarro (PN) energy landscape’. It is related to the PN potential, which reflects the fact that discreteness breaks the continuous translational invariance of a continuum model [37, 38]. The amplitude of the PN potential may be seen as the minimum barrier which must be overcome to translate an object by one lattice site. Regarding DBs, the Peierls-Nabarro barrier is given by the energy difference $|E_c - E_b|$, where E_c and E_b are the energies of a DB centered at a lattice site and between two lattice sites.

We define the Peierls-Nabarro energy landscape as follows: for a given configuration of amplitudes, A_n , the PN energy landscape is obtained by extremizing H with respect to the phase differences $\delta\phi_{ij} = \phi_i - \phi_j$:

$$H_{\text{PN}}^l = \min_{\delta\phi_{ij}}(-H) \quad ; \quad H_{\text{PN}}^u = \max_{\delta\phi_{ij}}(-H), \quad (13)$$

where $\psi_n = A_n \exp(i\phi_n)$ and H_{PN}^l and H_{PN}^u are the lower and upper part of the PN landscape. As we will see later, the bright breather solution $\vec{\psi}_{(x_3)}$ is located at an extremum of H_{PN}^l . The minus sign in the definition (13) was added for convenience to assure that the bright breather is found in a minimum (and not in a maximum) of the lower PN landscape. The phase differences extremizing the Hamiltonian

$$H = \frac{\lambda}{2}(A_1^4 + A_2^4 + A_3^4) - (A_1 A_2 \cos(\phi_1 - \phi_2) + A_2 A_3 \cos(\phi_2 - \phi_3)) \quad (14)$$

are $\delta\phi_{12} = \delta\phi_{23} \in \{0, \pi\}$. Hence, the upper and the lower PN energy landscapes read

$$H_{\text{PN}}^u = -\frac{\lambda}{2}(A_1^4 + A_2^4 + A_3^4) + (A_1 + A_3)A_2 \quad (15)$$

and

$$H_{\text{PN}}^l = -\frac{\lambda}{2}(A_1^4 + A_2^4 + A_3^4) - (A_1 + A_3)A_2. \quad (16)$$

In Fig. 2 the PN landscape is visualized for $\lambda = 3$. The PN ‘shell’, consisting of the upper and lower landscapes, bounds the phase space of the trimer. Since the DB whose properties we are studying corresponds to a minimum on H_{PN}^l , we shall focus on this landscape. As shown in Fig. 2 (c), the projection onto the $A_1 - A_3$ plane exhibits three minima which are separated by saddle points (called ‘rims’ in the following). For $\lambda \rightarrow \infty$ the saddle points are located at $A_1 = A_2 = \sqrt{1/2}$ (which in the following will be the saddle point of interest) and $A_2 = A_3 = \sqrt{1/2}$. The energy threshold E_{thrs} at the rim (obtained from Eq. (16)) reads

$$E_{\text{thrs}} = -\frac{\lambda}{4} - \frac{1}{2} - \frac{1}{4\lambda} + \frac{1}{4\lambda^2} - \frac{1}{4\lambda^3} + \frac{9}{16\lambda^4} + \mathcal{O}(\lambda^{-5}). \quad (17)$$

The following investigation holds for an effective non-linearity in a range around $\Lambda = \lambda/M \simeq 1$ [49], which is in the critical regime where scale-free avalanches of BECs were found in [28].

5. The Threshold for transfer of norm

To study the influence of the PN landscape on the stability and the transfer of atoms through the DB, we first consider the fixed point corresponding to the bright breather. The initial amplitudes A_i^b are obtained by inverting Eq. (7) for $N_2 > 1/2$; hence an initial condition for the bright breather reads $\vec{\psi}^b(0) = (-A_1^b, A_2^b, -A_1^b)$. Then perturbations are added to site 1. In dynamical systems terminology, the phase space of the trimer is ‘mixed’, consisting of regular islands surrounded by the chaotic sea [28, 39]. DBs are located inside the regular

islands of the phase space, provided that their frequency (and multiples of their frequency) lie outside the phonon spectrum [30, 31]. If a perturbation is large enough, it can push the orbit out of the regular island into the chaotic sea, destabilizing the DB.

We now use the following initial condition:

$$\vec{\psi}(0) = (-(A_1^b + \delta_A)e^{i\delta_\phi}, A_2, -A_1^b), \quad (18)$$

where $A_2 = (1 - |\psi_1|^2 - |\psi_3|^2)^{1/2}$ ensures total norm $N = 1$. Compared to the bright breather, we have added an amplitude δ_A to site 1 and the phase ϕ_1 is rotated by δ_ϕ . The initial condition (18) is visualized in Fig. 3(right panels), where we have fixed $\delta_\phi = \pi$ and increased δ_A in (a-d). Note that although the phase rotation does not alter the norms $|\psi_i|^2$, it drastically changes the total energy of the trimer which we define as $E_t = -H$ (see Eq. (14)).

In Fig. 3(left) we show the dynamics for increasing total energy E_t , where the arrows on the orbits (black curves) mark the direction of time. For $E_t < E_{\text{thrs}}$ the areas in phase space are disconnected, leading to sub-threshold dynamics depicted in Fig. 3a.

In contrast, for $E_t > E_{\text{thrs}}$ the orbit is allowed to pass the rim such that the majority of the norm migrates from site 2 to site 1 (Fig. 3b), while norm is transferred to site 3. The larger E_t (Fig. 3c), the larger is the size of the ‘bubble’ (by the term bubble we denote the accessible region of the PN landscape for $A_1 > 1/\sqrt{2}$). Hence, as we see from Fig. 3b-c(left), an upper limit to the norm that can possibly be transmitted through the DB can be read from the maximum value of A_3 inside the bubble

$$A_3^* = \max_{A_1 > 1/\sqrt{2}} A_3 \quad (19)$$

for fixed total energy E_t .

Finally, for even larger E_t , the orbit visits large parts of the phase space and large amplitudes $A_i(t)$ are found at all three sites, as depicted in Fig. 3d, where most of the orbit resides in the chaotic regime (Fig. 3d). In this case, no controlled shift of the DB from site 2 to 1 is observed and the DB becomes dynamically unstable. These dynamical instabilities can be associated with a (partial) depletion of the BEC [40, 41]; a detailed study of these effects is beyond the scope of our present investigation.

The upper bound A_3^* can be calculated analytically noting that for the projection onto the $A_1 - A_3$ plane, condition $dA_3/dA_1 = 0$ holds. Implicit derivation of Eq. 16 leads to

$$0 = 1 - 2A_1^2 - A_1 A_3 - A_3^2 + 2\lambda A_1 \sqrt{1 - A_1^2 - A_3^2} (-1 + 2A_1^2 + A_3^2), \quad (20)$$

that determines the maximum value of A_3 in the ‘bubble’

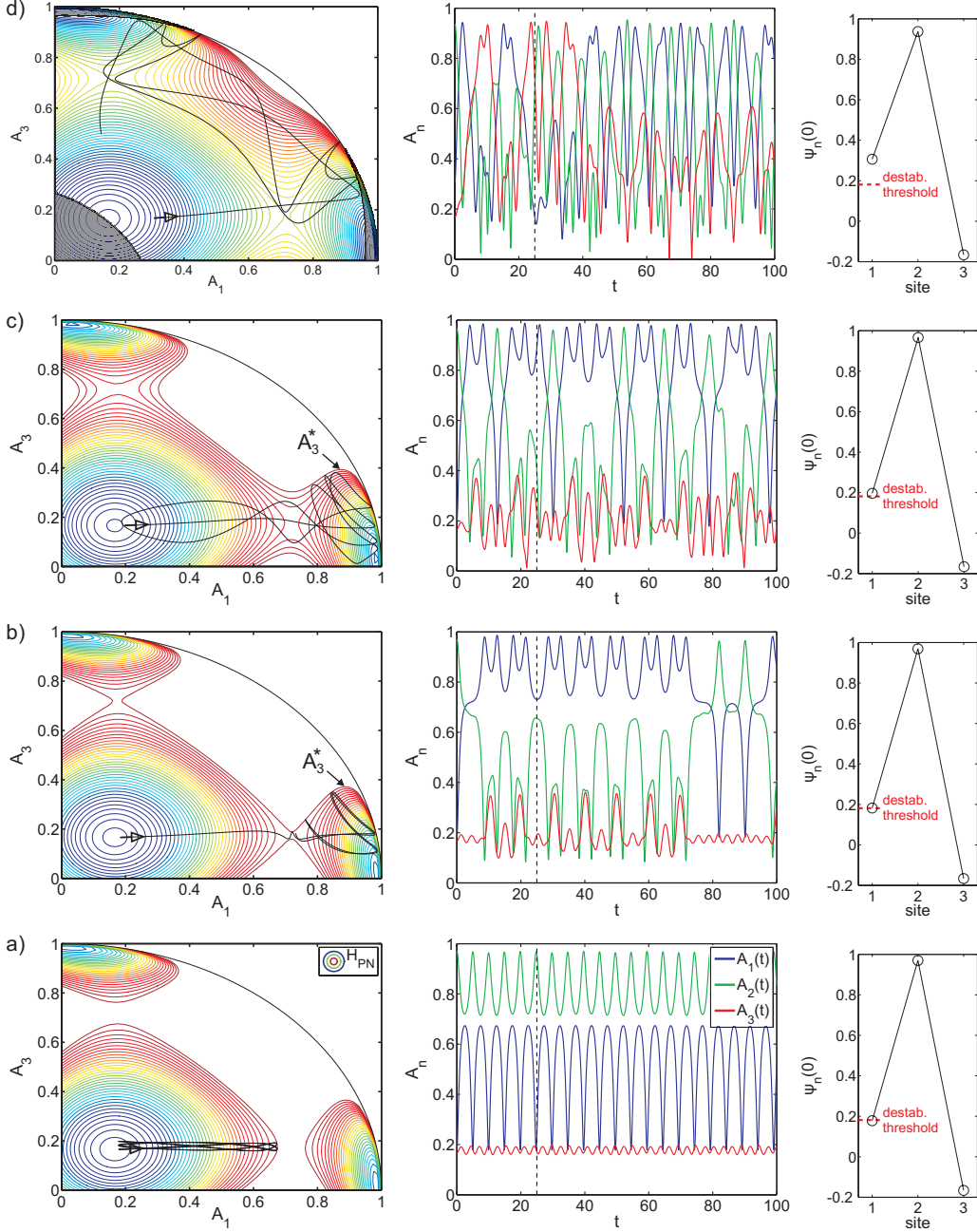


Figure 3: Dynamics on the PN landscape for increasing total energy of the trimer. **(a) (left)** A contour plot of the lower PN energy landscape H_{PN}^l is shown for total energy below the rim ($E_t = -1.32 < E_{\text{thrs}} = -1.311$). A projection of the orbit onto the A_1 - A_3 plane is over-plotted (black curve). **(middle)** The corresponding amplitudes $A_i(t)$ indicate that the maximum amplitude remains at the central site. The dashed vertical line marks the time interval $[0, 25]$ for which the orbits in the left picture are plotted. **(right)** A sketch of the initial condition shows that the excitation at site 1 is slightly below threshold. **(b)** Destabilization of the DB for $E_t = -1.310 > E_{\text{thrs}}$ just above the rim. We see that the rim of the PN landscape clearly restricts the dynamics and governs the destabilization process of the DB. **(c)** For higher total energy $E_t = -1.28$ the bottleneck at the rim widens and the maximum norm transmitted to site 3 is increased. **(d)** For even higher total energy $E_t = -1.04$ the orbit explores large parts of the phase space and visits all three sites. The grey shaded areas are forbidden by the upper PN landscape H_{PN}^u . In all cases $\lambda = 3$, $\delta_\phi = \pi$. For other values of δ_ϕ the same qualitative behavior is found.

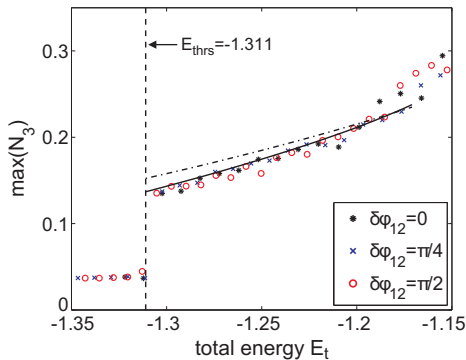


Figure 4: Norm transfer through a bright breather. The maximum (atomic) norm at site 3 detected after the collision of the DB with a lattice excitation is shown as a function of the total energy of the trimer. The discrete symbols indicate three different values of the initial phases. For $E_t < E_{\text{thrs}}$ the DB is stable and practically no transfer of norm takes place on short timescales. For $E_t > E_{\text{thrs}}$ we observe instability of the DB centered at site 2: The breather migrates to site 1 and norm is transferred to site 3. An upper bound to $\max(N_3(t))$ is calculated from the PN landscape, both analytically (dotted-dashed line, cf. Eq. (21)) and numerically (solid line). The analytical calculation is performed in the limit for large λ and therefore deviates slightly from the exact numerical result. We used $\delta\phi_{23} = \pi$ which is the typical case observed in [28] for DBs in an extended leaking optical lattice and $\lambda = 3$.

of the PN landscape as

$$\begin{aligned}
 A_3^*(\delta, \lambda) = & \frac{1}{\sqrt{2}} - \frac{\sqrt{(1-2\delta)}}{2\sqrt{\lambda}} - \frac{(1-2\delta)}{4\sqrt{2}\lambda} \\
 & + \frac{1+2(\delta-\delta^2)}{4\sqrt{1-2\delta}\lambda^{3/2}} - \frac{25-20(\delta-\delta^2)}{64\lambda^2} \\
 & + \frac{11/8-3\delta-\delta^2+7(\delta^3-7\delta^4)}{2(1-2\delta)^{3/2}\lambda^{5/2}} \\
 & + \mathcal{O}(\lambda^{-3}), \quad (21)
 \end{aligned}$$

where $\delta = E_t - E_{\text{thrs}} > 0$ is the energy relative to the destabilization threshold. Without the $\lambda^{-5/2}$ term the exact value is underestimated. If we truncate the expression after the $\lambda^{-3/2}$ term, the deviation from the exact result roughly doubles compared to what is shown in Fig. 4.

How general is the transfer mechanism that we describe? In Fig. 4, the maximum norm N_3 that is found at site 3 after the transfer of atoms through the DB is shown as a function of the total energy for three initial phase differences $\delta\phi_{12} = \pi - \delta_\phi = 0, \pi/4, \pi/2$. The dashed vertical line at $E_t = E_{\text{thrs}} = -1.311$ marks the total energy at the rim and is identified with the destabilization threshold of the DB. Evidently, the transfer mechanism found does not depend on parameters δ_A and δ_ϕ individually, but rather on the total energy which determines the accessible region of the PN landscape. Moreover, the transfer mechanism itself appears nearly

independent of the choice of the initial phase difference $\delta\phi_{12}$. The maximum norm detected at site 3 is closely below the upper bound $N_3^*(\delta) = |A_3^*(\delta)|^2$ given by Eq. 21 which holds for $E_t \lesssim -1.2$. For increasing $E_t \gtrsim -1.2$ the fluctuations of $\max(N_3)$ for different orbits with similar total energy become larger, because the orbits explore a larger part of the phase space. As a consequence, $\max_{t < T}(N_3(t))$ depends on the chosen time interval $[0, T]$ in which the maximum norm is detected (In all cases we set $T = 100$). In contrast, for lower total energy where a nontrivial upper bound $N_3^*(\delta)$ of the transferred norm holds, $\max_{t < T}(N_3(t))$ does barely depend on T already after very few oscillations of $A_3(t)$ (cf. Fig. 3b-c(middle)).

6. Connection to PN barrier

In order to gain further insight into the relation between the rim of the PN energy landscape and the PN barrier, let us consider a nonlinear trimer where we omit the nonlinear on-site interaction term at site 3. The equations of motion read

$$\begin{aligned}
 i\partial_t \psi_1 &= \lambda|\psi_1|^2\psi_1 - \frac{1}{2}\psi_2 \\
 i\partial_t \psi_2 &= \lambda|\psi_2|^2\psi_2 - \frac{1}{2}(\psi_1 + \psi_3) \\
 i\partial_t \psi_3 &= -\frac{1}{2}\psi_2. \quad (22)
 \end{aligned}$$

Using the initial condition (18) we find that on the timescale where the destabilization process of the DB centered at site 2 takes place, the dynamics is not changed substantially compared to the results for the nonlinear trimer (see Fig. 5). Hence, in order to describe the destabilization of the DB (and the basic mechanism of the norm transfer through the DB), it is sufficient to consider only two nonlinear sites with a third linear site attached. This is a strong indication that the destabilization threshold during the collision of the two objects can actually be linked to the Peierls-Nabarro barrier of a *single* DB.

7. Possible Applications

To start with, we would like to comment on the validity of the DNLS (3) to describe actual experiments of BECs in OLs. Experimental realizations have been performed for values of $\lambda = 2U/J$ in the range 10^{-5} – 10^{-3} , while the number of atoms is typically $N \sim \mathcal{O}(10^4 - 10^5)$. These estimations lead to experimentally feasible parameters $\Lambda = \lambda/M \lesssim 1$ for which the DNLS is a good approximation. For example, the experiment of [8] shows that the the BEC dynamics in an OL with parameters $N \approx 2 \times 10^5$, $J = 0.14E_R$, $2UN \approx 12E_R$ (where $E_R = \hbar^2 k_L^2 / (2m)$ is the recoil energy and k_L is the laser mode which traps the atoms), and $M = 200$ wells is described very well by the DNLS with effective nonlinearity

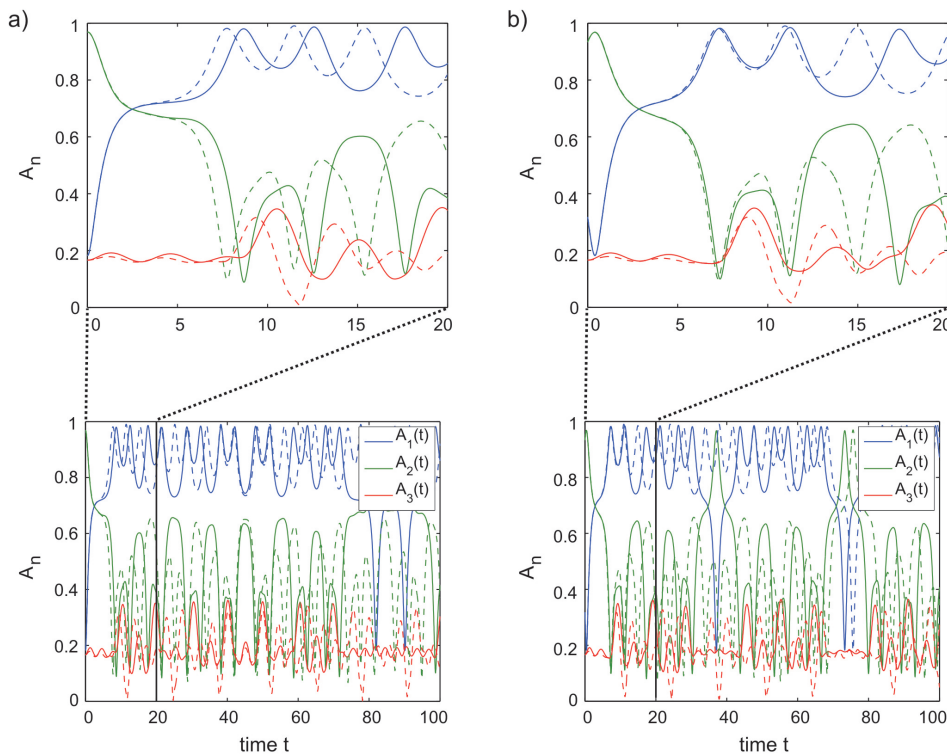


Figure 5: The destabilization of the DB in the trimer (solid line) is compared to the trimer with a third linear site (dashed line). On the timescale, where the destabilization takes place, the dynamics is qualitatively very similar (see enlargements in upper pictures). Total energy is $E_t = -1.31 > E_{\text{thrs}}$ and $\lambda = 3$. **(a)** The initial condition (18) is given by $\delta A = 0.016$, $\delta\phi = \pi$, which is the same as in Fig. 3b. **(b)** The initial condition is determined by the parameters $\delta A = 0.152$, $\delta\phi = \pi/2$.

$\Lambda \approx 0.5$. To estimate the minimum duration of an experiment with BECs probing the destabilization process, we rewrite our dimensionless time $t = J\tau$ in terms of real time τ . Typical values for J are taken from [42]: The Josephson energy $E_J/k_B = 378$ nK leads to the tunneling rate $J/\hbar = E_j(N\hbar)^{-1} = 16.5$ Hz (for $N = 3000$ atoms). Hence, with these parameters, $t = 10$ (which is a typical timescale after which the destabilization process took place) relates to $\tau \approx 0.6$ sec.

The thresholded transfer of norm through a bright breather that we analyzed may lead to interesting applications for blocking and filtering atom beams. It could be a powerful tool for controlling the transmission of matter waves in interferometry and quantum information processes [43].

In a similar way, our findings can be related to the field of optics, as the DNLS is capable of describing wave motion in nonlinear optical waveguide arrays. Discrete breathers in such two-dimensional networks were investigated in the past years both theoretically and experimentally [17, 18, 32–35, 44, 45] and can exhibit a rich variety of functional operations such as blocking, routing or logic functions [33, 34]. Experimental evidence of the destabilization process of the stationary DB should be observable in nonlinear waveguide arrays and might lead to functional operations such as filtering optical beams.

Moreover, in view of a molecular trimer, applications in terms of targeted energy transfer (introduced in [46, 47]) with a threshold are conceivable, e.g. in the field of biophysics or biomolecular engineering.

8. Conclusions

The threshold and the tunneling process during the collision of a DB with a lattice excitation (e.g. a moving breather) was described analytically by defining the 2-dimensional Peierls-Nabarro energy landscape. The PN landscape restricts the dynamics of the trimer and the accessible region of the phase space. This restriction of the dynamics becomes very pronounced at the destabilization threshold, which is identified with a rim in the PN landscape. The effect is found for a broad range of the phase difference $\delta\phi_{12}$ between the colliding objects.

Acknowledgments

The authors thank Boston University, where the bulk of this work was done, for hospitality and support. One of us (DKC) thanks the Max Planck Institute for Dynamics and Self-Organization for hospitality during the initial

stages of the project and the Aspen Center for Physics for hospitality during the completion of the work. We grate-

fully acknowledge useful conversations with Theo Geisel, Ragnar Fleischmann and Cristiane de Morais Smith.

-
- [1] M. H. Anderson, J. R. Ensher, M. R. Matthews, C. E. Wieman, and E. A. Cornell, *Science* **269**, 198 (1995).
- [2] O. Morsch and M. Oberthaler, *Rev. Mod. Phys.* **78**, 179 (2006).
- [3] I. Bloch, J. Dalibard, and W. Zwerger, *Rev. Mod. Phys.* **80**, 885 (2008).
- [4] T. Gericke, P. Würtz, D. Reitz, T. Langen, and H. Ott, *Nature Phys.* **4**, 949 (2008).
- [5] J. Estève, C. Gross, A. Weller, S. Giovanazzi, and M. K. Oberthaler, *Nature* **455**, 1216 (2008).
- [6] B. Eiermann, T. Anker, M. Albiez, M. Taglieber, P. Treutlein, K.-P. Marzlin, and M. K. Oberthaler, *Phys. Rev. Lett.* **92**, 230401 (2004).
- [7] I. Carusotto and G. L. Rocca, *Phys. Rev. Lett.* **84**, 399 (2000).
- [8] F. S. Cataliotti, S. Burger, C. Fort, P. Maddaloni, F. Minardi, A. Trombettoni, A. Smerzi, and M. Inguscio, *Science* **293**, 843 (2001).
- [9] M. Greiner, O. Mandel, T. Esslinger, T. W. Hänsch, and I. Bloch, *Nature* **415**, 39 (2002).
- [10] T. Schumm, S. Hofferberth, L. M. Andersson, S. Wildermuth, S. Groth, I. Bar-Joseph, J. Schmiedmayer, and P. Krüger, *Nature Phys.* **1**, 57 (2005).
- [11] D. K. Campbell, S. Flach, and Y. S. Kivshar, *Phys. Today* **57**, 43 (2004).
- [12] D. K. Campbell, *Nature* **432**, 455 (2004).
- [13] S. Flach and A. V. Gorbach, *Physics Reports* **467**, 1 (2008).
- [14] E. Trías, J. J. Mazo, and T. P. Orlando, *Phys. Rev. Lett.* **84**, 741 (2000).
- [15] A. V. Ustinov, *Chaos* **13**, 716 (2003).
- [16] M. Sato, B. E. Hubbard, A. J. Sievers, B. Ilic, D. A. Czaplowski, and H. G. Craidhead, *Phys. Rev. Lett.* **90**, 044102 (2003).
- [17] H. S. Eisenberg, Y. Silberberg, R. Morandotti, A. R. Boyd, and J. S. Aitchison, *Phys. Rev. Lett.* **81**, 3383 (1998).
- [18] R. Morandotti, U. Peschel, J. S. Aitchison, H. S. Eisenberg, and Y. Silberberg, *Phys. Rev. Lett.* **83**, 2726 (1999).
- [19] A. Xie, L. van der Meer, W. Hoff, and R. Austin, *Phys. Rev. Lett.* **84**, 5435 (2000).
- [20] U. T. Schwarz, L. Q. English, and A. J. Sievers, *Phys. Rev. Lett.* **83**, 223 (1999).
- [21] M. Sato and A. J. Sievers, *Nature* **432**, 486 (2004).
- [22] S. Aubry, *Physica D* **103**, 201 (1997).
- [23] A. R. Bishop, G. Kalosakas, K. Ø. Rasmussen, and P. G. Kevrekidis, *Chaos* **13**, 588 (2003).
- [24] J. Dornigac, J. C. Eilbeck, M. Salerno, and A. C. Scott, *Phys. Rev. Lett.* **93**, 25504 (2004).
- [25] G. P. Tsironis and S. Aubry, *Phys. Rev. Lett.* **77**, 5225 (1996).
- [26] K. Ø. Rasmussen, S. Aubry, A. R. Bishop, and G. G. Tsironis, *The Eur. Phys. J. B* **15**, 169 (2000).
- [27] R. Livi, R. Franzosi, and G.-L. Oppo, *Phys. Rev. Lett.* **97**, 4 (2006).
- [28] G. S. Ng, H. Hennig, R. Fleischmann, T. Kottos, and T. Geisel, *New J. Phys.* **11**, 073045 (2009).
- [29] R. Franzosi, R. Livi, and G.-L. Oppo, *J. Phys. B* **40**, 1195 (2007).
- [30] S. Flach and C. R. Willis, *Phys. Lett. A* **181**, 232 (1993).
- [31] S. Flach and C. R. Willis, *Physics Reports* **295**, 181 (1998).
- [32] D. Hennig and G. P. Tsironis, *Physics Reports* **307**, 333 (1999).
- [33] D. N. Christodoulides and E. D. Eugenieva, *Phys. Rev. Lett.* **87**, 233901 (2001).
- [34] D. N. Christodoulides, F. Lederer, and Y. Silberberg, *Nature* **424**, 817 (2003).
- [35] T. Kottos and M. Weiss, *Phys. Rev. Lett.* **93**, 190604 (2004).
- [36] A. Trombettoni and A. Smerzi, *Phys. Rev. Lett.* **86**, 2353 (2001).
- [37] Y. S. Kivshar and D. K. Campbell, *Phys. Rev. E* **48**, 3077 (1993).
- [38] B. Rumpf, *Phys. Rev. E* **70**, 9 (2004).
- [39] S. Mossmann and C. Jung, *Phys. Rev. A* **74**, 033601 (2006).
- [40] F. Trimborn, D. Witthaut, and H. J. Korsch, *Phys. Rev. A* **79**, 013608 (2009).
- [41] F. Trimborn, D. Witthaut, and H. J. Korsch, *Phys. Rev. A* **77**, 043631 (2008).
- [42] R. Gati, J. Esteve, B. Hemmerling, T. B. Ottenstein, J. Appmeier, A. Weller, and M. K. Oberthaler, *New Journal of Physics* **8**, 189 (2006).
- [43] R. A. Vicencio, J. Brand, and S. Flach, *Phys. Rev. Lett.* **98**, 184102 (2007).
- [44] Y. S. Kivshar, *Opt. Lett.* **18**, 1147 (1993).
- [45] J. Meier, G. I. Stegeman, Y. Silberberg, R. Morandotti, and J. S. Aitchison, *Phys. Rev. Lett.* **93**, 093903 (2004).
- [46] G. Kopidakis, S. Aubry, and G. P. Tsironis, *Phys. Rev. Lett.* **87**, 165501 (2001).
- [47] G. P. Tsironis, *Chaos* **13**, 657 (2003).
- [48] Indications for the migration of a DB by one or a few sites towards a lattice excitation can be found as well in a ϕ^4 nonlinear lattice; see M. Ivanchenko, O. Kanakov, V. Shalfeev and S. Flach, *Physica D* **198**, 120 (2004).
- [49] For nonlinearities $\Lambda \ll 1$ no such saddle points in the PN landscape are found.